ACCSCIENCE PUBLISHING

Materials Science in Additive Manufacturing

REVIEW ARTICLE

Porosity and density measurement of additively manufactured components: A comparative analysis of measurement methods across processes and materials

Erik Westphal[1]* and Hermann Seitz[1,2]

[1]Chair of Microfluidics, University of Rostock, Rostock, Germany

[2]Department of Life, Light & Matter, University of Rostock, Rostock, Germany

Abstract

Part density and part porosity are important parameters for additively manufactured (AM) components, as they significantly influence mechanical properties and indicate printing process's quality. Various measurement methods are available such as gas pycnometry, gravimetric density measurements (Archimedes' principle), and micrograph analyses. This study compared these methods by analyzing test specimens made from different materials using diverse AM processes. AM components made of metal, ceramic, and plastic as well as composites were analyzed with regard to part density and porosity. The results provided new findings on part density and porosity in AM processes and materials. Furthermore, they demonstrated the suitability of the employed measurement methods for certain purposes. In this context, it is always important to distinguish between the determination of true and apparent density. Gas pycnometry is best suited for determining the true density and enables the most accurate density measurement. Gravimetric measurement according to Archimedes' principle is generally best suited for determining the apparent density, which is more relevant for characterizing the technical properties of AM components. Micrograph analyses are the only investigated method that shows the position of the pores in the component. However, the method generally only allows statements to be made in the sectional plane under consideration. In addition, gas pycnometry is preferable for very dense AM components and the Archimedes method for porous parts. Finally, the results can be generalized and recommendations for measuring porosity and density can be concluded for other AM processes.

Keywords: Additive manufacturing; True density; Apparent density; Open porosity; Closed porosity

***Corresponding author:**
Erik Westphal
(erik.westphal@uni-rostock.de)

Citation: Westphal E, Seitz H. Porosity and density measurement of additively manufactured components: A comparative analysis of measurement methods across processes and materials. *Mater Sci Add Manuf.* 2025;4(2):025090010. doi: 10.36922/MSAM025090010

Received: February 27, 2025

Revised: March 27, 2025

Accepted: April 7, 2025

Published online: May 7, 2025

1. Introduction

Additive manufacturing (AM) is a manufacturing technology for the layer-by-layer creation of objects from three-dimensional (3D) model data. The technology is divided into seven different process categories according to International Organization for Standardization (ISO)/American Society for Testing and Materials (ASTM) 52900.[1] Table 1 provides an

overview of the individual process categories and their technological advantages and disadvantages.

AM technologies utilize different principles to process a wide range of materials. In this study, four AM processes with different printing materials are analyzed as examples, which are characteristic for the broad spectrum of AM processes and materials with regard to the results of the 3D printing process. In the first process examined, the material extrusion (MEX) process, a thermoplastic filament is applied layer by layer to a build platform by softening and localized application via a heated nozzle. The process is also known as fused deposition modeling (FDM)[3] and can also produce metallic components, for example from 316l stainless steel, in a two-stage production process consisting of the actual printing and a subsequent debinding and sintering step.[4] In powder bed fusion (PBF), an energy source is used to locally sinter or fuse a powdered material. In the second process studied, selective laser sintering (SLS), a laser is used to sinter polyamide 12 (PA12) powder whereas in the third examined process, electron beam melting (EBM), an electron beam is used to produce metallic components by completely melting titanium powder. VAT photo-polymerization (VPP) is a

Table 1. Additive manufacturing process categories according to published literature[1,2]

Process category		Definition	Advantages	Disadvantages
Binder jetting		AM process in which a liquid binder is selectively applied to powder materials to cause them to bond	Wide range of materials, low powder consumption, high productivity, no support structures, high speed	Multi-stage process, extensive post-processing, high porosity, low strength
Directed energy deposition		AM process that uses focused thermal energy to fuse materials together during deposition	Production of large parts, fast repair of metal parts, high process speed, low waste	Low resolution and poor surface quality, no support structures, limited design freedom
Material extrusion		AM process in which materials are selectively applied through a nozzle or orifice	Simple and familiar process, wide range of materials, cost-effective, mechanically resilient components	Low resolution and production accuracy, poor surface quality, a lot of post-processes, slow production process
Material jetting		AM process in which drops of the starting material are applied in a targeted manner	High-precision process, good material combination, low material loss, high density and strength	Low process speed, increased post-processing effort, poor mechanical resilience, expensive
Powder bed fusion		AM process in which thermal energy selectively melts areas of a powder bed	High density and strength, high precision, great design freedom, good mechanical properties and load-bearing capacity	Relatively slow and expensive, limited material variety, high process costs, poor powder recycling, limited surface quality
Sheet lamination		AM process in which sheets of material are joined to form a component	Fast process, suitable for large components, simple technology	Niche process, a lot of post-processes, little material variety, strong anisotropy of the components, high level of wastage
VAT photo-polymerization		AM process in which liquid photopolymer is selectively cured in a bath by light-activated polymerization	Very high accuracy, smooth surfaces, low material consumption	Necessity of support structures, brittle components, ultraviolet post-curing if necessary

Abbreviation: AM: Additive manufacturing.

process in which an ultraviolet (UV)-sensitive polymer resin is used as a printing material and cured layer by layer using UV light. The fourth process chosen was lithography-based ceramic manufacturing (LCM) as a representative of the VPP processes, which can produce ceramic components, *for example*, from zirconium oxide, by light-curing a ceramic-loaded slurry and then debinding and sintering the green body.[5]

All components manufactured using the respective AM processes have characteristic properties that make them suitable for applications of varying complexity. The applications range from low-stress prototypes to final components that are sometimes exposed to high loads. With increasing stress on AM components, it is important to be able to evaluate the manufacturing quality of the structures. The density and porosity of AM components are of great interest here, as they have a strong influence on the mechanical properties and are the most economical to analyze.[6-8] Porosity in this case is the presence of a defect in the form of a pore or cavity or a lack of solid material in the fractions of a component.[9] A certain degree of porosity cannot be avoided in any AM process, meaning that internal pores are always present in every AM component.[6,10-12] According to the ASTM, porosity in AM can be categorized into two main types: apparent porosity (unintentionally occurring defects in the structure and/or surface of AM material) and artificial porosity (intentionally created and controlled to enable a specific performance or function).[13] The apparent porosity has a negative influence on the mechanical component properties and the corresponding pores often act as nuclei for fatigue cracks.[10,12,14,15] Heavily stressed components should therefore have the lowest possible apparent porosity and be completely sealed to minimize the probability of failure during operation.[6] For certain biomedical implants, on the other hand, a certain degree of (artificial) porosity is desired, for example, to promote better osseointegration with biological tissue.[7,11,16]

Various non-destructive methods such as the Archimedes method, gas pycnometry, and X-ray computed tomography (CT), as well as destructive methods such as micrograph analysis or mercury intrusion (Hg intrusion), are suitable for investigating and quantifying the porosity of AM components and its effects on the mechanical component properties.[6,17] All of these methods are based on the detection of microstructural defects and pores in the components and, in some cases, on the analysis of porosity distribution.[12] Furthermore, all methods have specific measurement characteristics or manual influences that affect the measurements to a certain extent and thus lead to deviations between the measurement results.[6] In addition, some processes are very complex, time-consuming, or, as in the case of Hg intrusion, pose environmental and health risks due to the use of toxic substances. An extensive comparison of the individual measurement methods for different AM components made of metal (titanium printed using PBF and stainless steel printed using MEX), ceramic (ZrO_2 produced using VPP), and plastic (PA12 produced using PBF) with regard to their part density and porosity using automated measurement methods and processes has not yet been carried out. In addition, AM ceramic and metal green parts (composites) produced using VPP and MEX, respectively, are also analyzed, and thus the accuracy and reproducibility of the respective measurement methods are evaluated at an early stage of a multi-stage AM production process. This is the subject of the present work. As a result of the investigations, conclusions are then drawn about the preferred density measurement methods for various AM processes.

2. State of the art

In the state-of-the-art, basic principles of pores and porosities, as well as densities of components, are first explained. Furthermore, special measurement methods are considered. Current research on the density and porosity of AM components, which were determined using the analysis methods investigated in this study, are then discussed. Data from other literature are of comparative significance to the results of this study.

2.1. Principle of open and closed pores

Many parts do not consist entirely of a solid component but have cavities, capillaries, and inclusions. According to Otto *et al.*,[18] these cavities can be filled with air or any single-phase or multiphase liquid and consist of several areas, so-called pores. According to ISO 15901-1,[19] these pores are in turn divided into closed and open pores. According to Klobes and Munro,[20] this classification is based on how accessible they are to an external fluid (Figure 1). Closed pores are inaccessible to an external fluid and are also

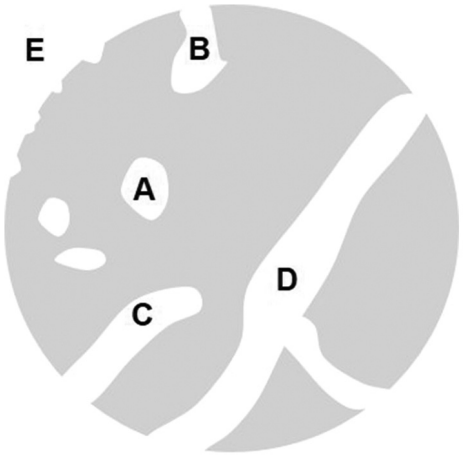

Figure 1. Schematic representation of closed (A) and open (B-D) pores and the surface roughness (E) of a component (based on Klobes *et al.*[20])

completely isolated from other pores (Figure 1A). These pores influence the macroscopic properties of bulk density, elasticity, mechanical strength, and thermal conductivity of a part.[18,20] Open pores, on the other hand, have either one opening (blind pores) or several openings (continuous pores) or connections to the outer component surface (Figure 1B-D) and enable exchange with the environment through media flow.[18,20] In the case of pores, it should also be noted that, by definition according to ISO 15901-1, they must also be deeper than wide to be categorized as pores. Otherwise, according to Klobes and Munro,[20] corresponding areas are more likely to be categorized as surface roughness (Figure 1E).

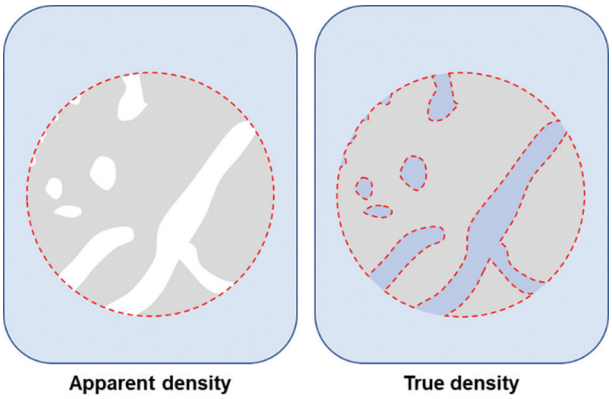

Figure 2. Difference between apparent and true density

2.2. Determination of material density and porosity

When considering a component with or without its closed pores, there are differences in terms of density and porosity. Apparent density is referred to when the total volume of a component including all (open and closed) pores is considered (Figure 2, left). The apparent density is calculated by dividing the part mass by the total volume (including the pores). If the pores are not considered when measuring the density, this is referred to as the true density (Figure 2, right). It is calculated by dividing the part mass by the part volume without pores. The difference between apparent and true density indicates the porosity of the material.

There are different measurement methods for measuring the individual types of density. Gravimetric density measurement according to Archimedes' principle includes the trapped air in the component and is therefore very suitable for apparent density, while, for example, gas pycnometry largely displaces the trapped air from the component and is therefore more suitable for determining true density. This is due to various properties such as the existing pore size, the structure of the pores, and the material density, which influence the reliability of a measurement. Figure 3 shows further measurement methods that characterize certain pore sizes and provide conclusions about the part density and part porosity. Table 2 then describes the advantages and disadvantages of the individual methods with regard to the determination of part density and porosity.

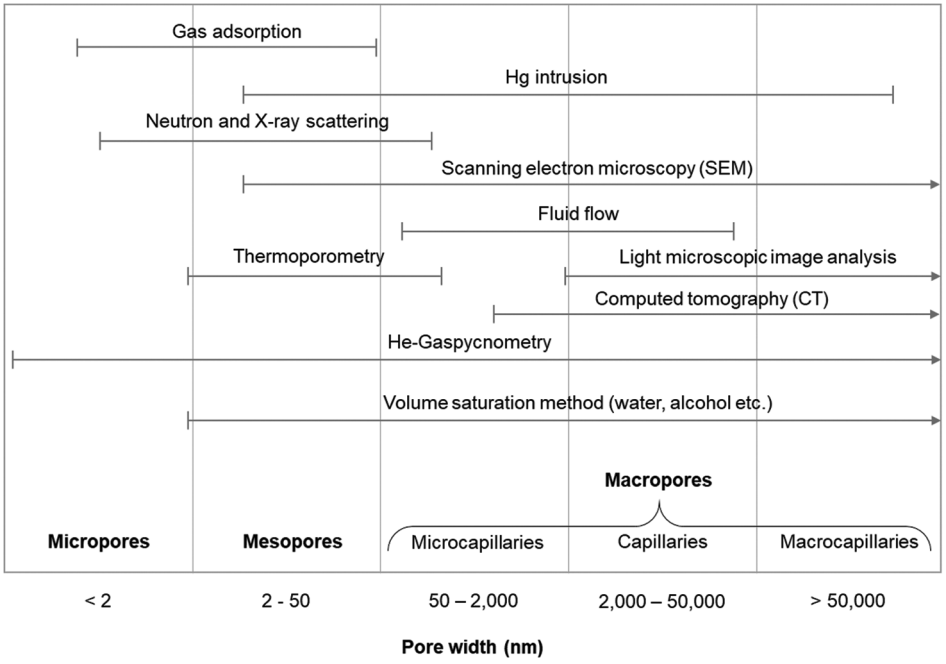

Figure 3. Limits of different pore size measurement methods (according to Klobes *et al.*[20])

Table 2. Methods for determining the open or total porosity depending on the pore size.

Procedure	Pore size range (nm)	Porosity measurement	Density measurement	Advantages	Disadvantages
Gas adsorption	<50	Indirect	Indirect	Allows for specific measurement of surface area and pore size; provides additional information on porosity	No direct determination of porosity and density; closed pores not measurable
Mercury intrusion	4 – 60,000	Direct	Indirect	Covers large pore area, direct measurement of open porosity and indirect measurement of apparent density above it	Hazardous to health and environment; destructive process; closed pores not measurable
Neutron and X-ray scattering	1 – 100	Indirect	Indirect	Examination of the part structure at atomic level; allows conclusions to be drawn about porosity and density	Very complex, expensive procedure; radiation exposure
Scanning electron microscope	>10	Direct	Indirect	High resolution and depth of field for qualitative pore information	High costs and labor-intensive; no direct density measurement
Light microscopic image analysis	>2,000	Direct	Indirect	Measurement of open and closed pores; wide application for many materials	Only local porosity measurement; complex; no direct density measurement
Computed tomography	>1,000	Direct	Direct	Non-destructive density and porosity analyses; spatial resolution and 3D imaging	Only radiolucent materials measurable; expensive; time-consuming
Helium gas pycnometry	>1	Indirect	Direct	Very fast measurement, good reproducibility; non-destructive; highly accurate	No determination of pore distribution; limited sample size; closed pores cannot be measured
Volume saturation method	>2	Direct	Indirect	Simple and inexpensive measurement of open pores; non-destructive and accurate	No determination of pore distribution; time-consuming and slow; closed pores cannot be measured
Archimedes method	>100	Indirect	Direct	Simple and fast measurement; non-destructive; complex samples can be measured	Inaccurate with very small or porous samples; influenced by surface tensions; closed and small open pores cannot be measured

When determining density and porosity, a distinction must be made between direct and indirect measurement methods. Direct porosity measurement methods aim to determine the porosity by direct measurement of the pore structure, *for example*, by imaging methods (light microscopic image analysis, CT, scanning electron microscope analysis) or mercury intrusion. Indirect measurement methods determine the porosity by measuring another physical part property, such as density, and then calculate the porosity from this, *for example*, using gas pycnometry, volume saturation methods, or gravimetric density measurement methods based on Archimedes' principle. This density measurement method, also known as the Archimedes method, is also a direct measurement method for determining the (apparent) part density. Neutron and X-ray scattering are indirect methods for determining porosity, as they provide information about the structure of the material at an atomic or molecular level and then allow conclusions to be drawn about the porosity. Gas adsorption is also an indirect measurement method that measures the specific surface area and pore size of components and provides additional information for characterizing porosity.

2.3. Porosity evaluations of AM structures

Within the scope of the materials for AM components examined in this study, manual density measurements according to Archimedes, specific micrograph analyses, and investigations with the gas pycnometer to determine density and porosity were most frequently documented.[6,7,17,21,22]

Damon *et al.*[23] carried out porosity tests specifically on FDM-printed parts made of 316L stainless steel. The sintered parts were analyzed with the help of micrographs, among other things. During the tests, a porosity of the parts of 0.5 – 1.7% was determined, whereby a part density of the sintered 316L components of up to 99.5% can be achieved. The microstructure and pore structure of the components were also analyzed using micrographs. However, the porosity of the parts was not validated using other analytical methods, and the unsintered 316L green parts were not analyzed.

Gong *et al.*[24] investigated the density of sintered 316L FDM parts using a gas pycnometer and micrograph analysis. A part density of 7.88 g/cm³ was measured for

the sintered 316L components and a part porosity of approximately 1.5% was determined. The results were not validated with further density or porosity analyses, nor were any tests carried out on the 316L green parts.

The mechanical and geometric properties of FDM-printed components made of 316L stainless steel were also characterized by Caminero *et al.*[25] Among other things, the part density and porosity were determined using the Archimedes method and the pore distribution by micrograph analyses. For sintered 316L component samples, a porosity of 1.9 – 2.1%, depending on the component orientation, was documented. The results were not validated by other analytical methods or by analyzing 316L green parts.

Dupin *et al.*[22] analyzed the density and porosity of SLS parts made from various PA12 powders using the Archimedes method. In addition, the microstructure of the parts was mapped using micrograph analyses. At a laser power of 10 W, a porosity rate of approx. 6.1 – 6.5% was determined using the Archimedes method.

Porosity evaluations on parts made of titanium powder using EBM were carried out by Galarraga *et al.*[26] using micrograph analysis. A maximum part porosity of 0.25% was measured. The part density was not determined and the porosity results were not validated using other analytical methods.

Scharowsky *et al.*[27] also analyzed the porosity of EBM parts made of titanium by micrograph analysis. A part porosity of 0.17% was determined for optimized system settings. No further porosity or density analyses were carried out.

The density of sintered zirconium oxide ceramic produced using the LCM process was determined by Homa and Schwentenwein[28] using the Archimedes method. A part density of 6.011 g/cm³ was measured. No further comparative analyses were carried out. In addition, the green parts were not analyzed.

Llanos[29] used micrograph analyses to determine the density and porosity of sintered zirconia ceramics printed using the LCM process. Part densities of 6.01 – 6.02 g/cm³ and part porosities of 0.98 – 1.18% were determined.

In addition, Suominen *et al.*[30] also determined the density of LCM-printed zirconia ceramics using the Archimedes method. Part densities of 6.022 – 6.085 g/cm³ were measured. Comparative analysis methods were not used and green parts were not analyzed.

A summary of the density and porosity values determined in the literature for parts manufactured using the same AM materials and processes as in the present study is given in Table 3.

3. Materials and methods

To quantify the influence of the component geometry on the analysis quality of the density and porosity measurement methods, three components of varying complexity (cuboid, cylinder, femoral ball head) were designed using the Computer-Aided Design software Autodesk Inventor Professional 2019 (Autodesk Inc., San Rafael, USA) (Figure 4). The component files were then exported as STL files and prepared for printing using the four AM processes selected. The dimensions of the component designs are listed in Tables 4 and 5.

Table 3. Part density and porosity of various AM materials and processes

Method	Material	Porosity (%)	Density	Analysis method	Source
FDM	316L green	-	4.3 – 4.6 g/cm³	Calculation of weight/volume	31
FDM	316L green	1.7	4.46 – 4.73 g/cm³	Micrograph analysis	32
FDM	316L sintered	1.5	7.88 g/cm³	Gaspycnometer	24
FDM	316L sintered	1.9	-	Archimedes method	25
SLS	PA12	4.1 – 6.7	-	Archimedes method	22
EBM	Titan	0.25	-	Micrograph analysis	26
EBM	Titan	0.17	-	Micrograph analysis	27
LCM	ZrO_2 slurry		2.89 – 3.32 g/cm³	Calculation of weight/volume	33
LCM	ZrO_2 sintered	-	6.011 g/cm³	Archimedes method	28
LCM	ZrO_2 sintered	0.98 – 1.18	6.01 – 6.02 g/cm³	Micrograph analysis	29
LCM	ZrO_2 sintered	-	6.022–6.085 g/cm³	Archimedes method	30

Abbreviations: AM: Additively manufactured; EBM: Electron beam melting; FDM: Fused deposition modeling; LCM: Lithography-based ceramic manufacturing; SLS: Selective laser sintering.

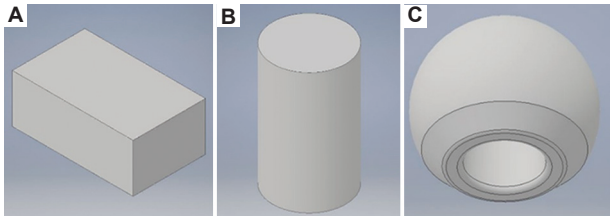

Figure 4. Computer-aided designs of the test components: (A) Cuboid, (B) cylinder, and (C) femoral ball head

Table 4. FDM process parameters and part dimensions for printing.

Parameter	Cuboid	Cylinder	Femoral ball head
Extruder temperature (°C)		235	
Print speed (mm/s)		10	
Infill density (%)		100	
Heater chamber temperature (°C)		80	
Layer height (mm)		0.14	
Support	**Raft**	**Raft**	**Brim**
Part dimensions (mm)	15×15×20	Ø15×20	Ø32

Table 5. LCM process parameters and part dimensions for printing

Parameter	Cuboid	Cylinder	Femoral ball head
DLP energy (mJ/cm²)		100	
DLP intensity (mW/cm²)		73.8	
Setting time (s)		4	
Tilting speed (°/s)		15	
Layer height (mm)		0.025	
Support	-	-	**Raft**
Part dimensions (mm)	10×10×10	Ø10×10	Ø16

Abbreviation: DLP: Digital light processing.

3.1. AM processes

3.1.1. MEX (FDM)

A Makerbot Method X desktop 3D printer (MakerBot Industries LLC, Brooklyn, USA) was used for the FDM process. Furthermore, a 0.4 mm nozzle and a heated build chamber were used for printing. The metal-polymer composite filament Ultrafuse 316l (BASF SE, Ludwigshafen, Germany) was used as the printing material. The filament contains a metal powder content of 80 wt% with a filament diameter of 1.75 mm. The STL files of the part designs were prepared for printing using the slicer software Makerbot Print (MakerBot Industries). The relevant process parameters set in MakerBot Print and the component dimensions are summarized in Table 4. All components were printed individually.

After printing, green parts were initially available, which were analyzed with regard to their density and porosity. The green parts were then subjected to a catalytic debinding and sintering process. This was carried out externally by a sintering service provider recognized by the material manufacturer (Elnik System GmbH, Waldachtal, Germany) and in accordance with the specifications defined by the material manufacturer.[34] After this process, the components consist entirely of 316L stainless steel.

3.1.2. PBF (SLS)

An S2 laser sintering system (Sintratec AG, Brugg, Switzerland) was used for the SLS process, in which powdered PA12 (Sintratec AG) was processed. The SLS printer is equipped with a 10 W diode laser, which has a laser wavelength of 1064 nm. The laser spot size was 145 µm and the scan speed 3 m/s. A value of 0.1 mm was preset for the layer thickness. The build chamber was heated to 180°C during the printing process. The apparent powder density of the PA12, determined using a gas pycnometer (Section 3.2), was 1.065 g/cm³. The Sintratec Central2 slicer (Sintratec AG) was used to prepare the components. All components were printed in a single printing process and had the same dimensions as the FDM-printed green parts. After the printing process, the components were cleaned and the residual powder was removed by blasting with glass beads. The components were then analyzed.

3.1.3. PBF (EBM)

The EBM components were manufactured using an A1 EBM system (Arcam SE/GE Additive, Mölndal, Sweden). Titanium powder Ti6Al4V (Arcam SE) with an apparent powder density of 4.433 g/cm³ determined by gas pycnometry (Section 3.2) was also used. The process parameters of the production process were set internally on the system. The layer thickness was 0.05 mm, maximum beam current 39.5 mA, hatch spacing 0.05 mm, and scan speed 800 – 11279 mm/s. The components were prepared using Autodesk Netfabb (Autodesk Inc., San Rafael, USA). All components were printed in one printing process and had the same dimensions as the FDM-printed green parts and the SLS components. After printing, the components were removed from the building platform and cleaned by sandblasting. These post-processing steps were followed by the analyses.

3.1.4. VAT photopolymerization (LCM)

LCM components were printed using a CeraFab 7500 system (Lithoz GmbH, Vienna, Austria). A digital light processing principle was used. A photoreactive suspension (slurry) of methacrylates and zirconium powder (Lithoz) was used as the print material type. The zirconium powder

loading was 45% by volume. The components were prepared using Autodesk Netfabb and the process parameters set on the printer are listed in Table 5. Three print jobs were carried out in which all components of a design were produced.

After printing, green parts were available, which were first washed in isopropanol and analyzed for density and porosity. One green part of each design was then subjected to a sintering process. The sintering process was carried out in-house according to a Lithoz specification.[35] A sintering furnace (Nabertherm GmbH, Lilienthal, Germany) was used for sintering, which could automatically run the predefined sintering ramps.

3.2. Density and porosity measurement

3.2.1. Gas pycnometry

The gas pycnometer measurements were carried out using an Ultrapyc 5000 gas pycnometer (Anton Paar GmbH, Graz, Austria) and helium. With this measurement, the true density of component samples (or the material density of powder) can almost be determined by volume. The open porosity of a sample can also be measured. For this purpose, a sample is placed in a primary container with a calibrated and precisely known volume at atmospheric pressure. This container is then filled with helium up to a certain pressure P1. The gas is then expanded to a defined pressure P2 in another empty expansion vessel with a known volume at atmospheric pressure. The pycnometer measures the volume of displaced gas from the primary container at pressure P1 to the expansion container up to pressure P2. The change in pressure enables the sample volume to be determined. The helium is forced into the pores and channels of the component by pressure and displaces the air normally contained therein. Only completely closed pores and pores with a diameter of <1 nm cannot be flushed by the helium and continue to contain air, which leads to measurement uncertainties in the density determination. However, these are very low with helium gas pycnometry. The density and porosity of the component can then be calculated using the mass of the tested sample, which was determined using a balance before the analysis, and the determined sample volume. For the investigations in this work, five consecutive measurements were carried out for each component sample in airtight containers to reduce the influence of measurement uncertainty.

3.2.2. Archimedes method

The fully automated Density L system (Dimensionics GmbH, Kessin, Germany) was used to measure density according to Archimedes' principle. During the measurement, the weight and volume of a body in air and in a liquid are measured and the buoyancy force acting on the body immersed in the liquid is equated with the weight of the amount of liquid displaced. The method is also known as gravimetric density measurement according to Archimedes' principle and is often used with special measurement setups and manual measurement procedures. It is suitable for determining the apparent density of a component and for determining its open porosity. As with gas pycnometry, gravimetric measurement according to Archimedes's principle also attempts to reduce the influence of the air trapped in the components. Due to capillary effects and the larger molecules of water compared to helium, only larger open pores in the surface layers of the components can be infiltrated. This means that the air still trapped in the component pores leads to buoyancy, which in turn influences the density measurement. The measured density is generally lower than that measured with gas pycnometry. However, the measurements are highly dependent on the measurement procedure and the human influence factor.

Due to a high degree of automation, the automated Density L measuring system used virtually eliminates the human influence factor during measurement. Furthermore, environmental parameters such as air pressure and temperature are recorded through sensors and included in the density determination using integrated software and correlation equations. This enables the fully automated measuring system to achieve a very high measuring accuracy of up to 0.001 g/cm³.

In this study, each sample was measured three times automatically. Except for the PA12 samples, all samples were measured in distilled water with 0.2% BYK-DYNWET 800 N surfactant (BYK-Chemie GmbH, Wesel, Germany). The PA12 samples were measured in ethanol ≥99.5% to avoid floating of the lightweight plastic components. Air pressure, air temperature, and fluid temperature were recorded by sensors for each measurement and considered in the density calculation. Between the individual measurements, the samples were dried to evaporate the water trapped in the open pores and thus not falsify the subsequent measurements.

3.2.3. Micrograph analysis of cross-sections

For micrograph analyses, the component samples were separated, embedded in KEM 90 epoxy resin (ATM Qness GmbH, Mammelzen, Germany), ground (grit 1200 to 4000), and polished with a diamond suspension (ATM Qness). Two polished samples were created for each printed component, one horizontal and one vertical to the build direction. A BX51 light microscope (Olympus K.K., Shinjuku, Japan) was then used to generate the digital micrographs. For each micrograph, five measuring fields were examined at defined positions (Figure 5) with a magnification of 33.5×. The component porosity was then determined using the mean value of the individual measurement field porosities. In contrast to gas pycnometry and the Archimedes method, this method determines the

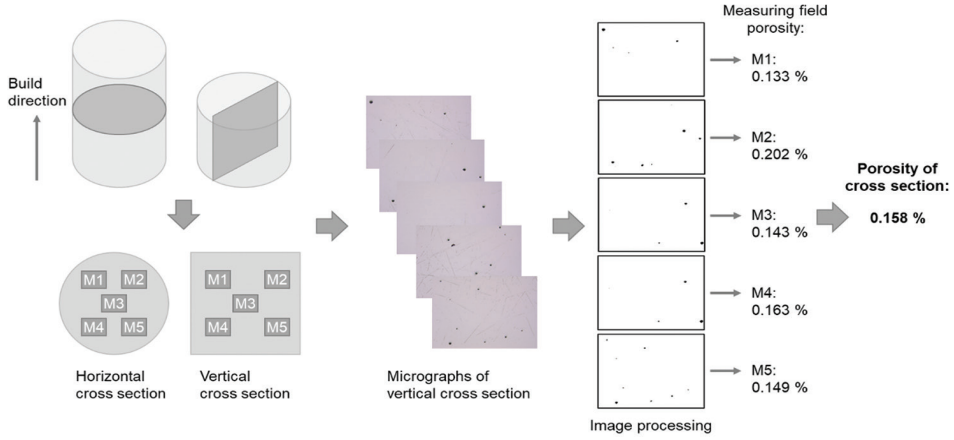

Figure 5. Micrograph analysis for porosity measurement of an additively manufactured titanium part

total porosity, whereby closed pores are also included in the calculations for the first time. However, only those pores that lie in the respective sectional plane under consideration and are larger than approximately 2 µm are included. Accordingly, a micrograph analysis is not representative for the entire component, but only for the considered plane and the examined measuring fields.

The recorded micrographs were analyzed with the image processing software ImageJ version 1.53k (Wayne Rasband and contributors, National Institutes of Health, USA). The individual cross-sections of the measurement fields were first converted into a black-and-white binary image, with black areas representing pores or other irregularities. By setting special shape, size, and quality parameters, irregularities in the binary image such as scratches, breakouts, and dirt were then automatically removed. The analysis of the binary images then ultimately provided the percentage of the area of the black pixels in the measurement field in relation to the total number of pixels. It should be noted that the microsection analysis provides a porosity rate and not a density as with the Archimedes method or gas pycnometry.

3.3. Standards and calculation methods used

For AM, ISO/ASTM 52927, the currently valid standard, provides recommendations for the use of test methods for various base materials. Accordingly, the density determination for AM metal components should be carried out according to ISO 3369, for plastic components according to ISO 1068, and for ceramic components according to ISO 18754. In this work, ISO 3369 was used as the basis for all investigations to enable uniform processes and documentation as well as directly comparable results.

The density values of the components for the gas pycnometer and buoyancy measurements according to Archimedes method were taken from the respective analyzers. The total porosity was calculated according to prior literature[22] using Equation I:

$$\text{Porosity} = \left(1 - \frac{\rho_P}{\rho_{theo}}\right) * 100 \quad \text{(I)}$$

The calculation is based on the determined density of the examined component ρ_p and the theoretical density ρ_{theo} of the respective component material. The theoretical density values of the materials used in this work were taken from the respective material data sheets or literature or determined using a gas pycnometer. However, the values determined only represent an actual state for the analyzed component or material and the respective measurement and may change due to altered measuring conditions, other material batches or other operator influences. This can lead to systematic errors, which are not discussed further in this paper. The theoretical component and measured material densities are listed in Table 6.

In the micrograph analyses, the part porosity in the section plane is first determined as described. The relative part density is then determined from this. However, the density ρ_p can also be calculated directly from the porosity by converting Equation I to Equation II:

$$\rho_P = \rho_{theo} \times \left(1 - \left(\frac{Porosity}{100}\right)\right) \quad \text{(II)}$$

4. Results and discussion

4.1. Visual inspection, density, and porosity characterizations

After the individual printing processes, the resulting component quality of the individual test samples was first visually inspected with regard to irregularities and surface quality. The part density and porosity were then determined. The components were first examined using a gas pycnometer.

Table 6. Theoretical and measured density values of the printing materials used in this work

Material	Condition	Density (g/cm³)	Source
316L	316L composite	5.000	Helium pycnometer measurement of the 316L filament
316L	Full material	8.000	AISI type 316L stainless steel[24]
PA12	Powder	1.065	Helium pycnometer measurement of the powder
Titan	Powder	4.433	Helium pycnometer measurement of the powder
ZrO_2 green part	ZrO_2 slurry	3.715	Helium pycnometer measurement of a reference ZrO_2 green part from the same material batch and printing setup
ZrO_2 sintered	Full material	6.088	Technical data sheet[36]

The density was determined and the porosity was calculated indirectly using the theoretical density of 316L stainless steel from Table 6 in accordance with Equation I. In comparison, the density of the same components was then measured fully automatically according to Archimedes' principle, and the porosity was again determined indirectly according to Equation I. Finally, further comparative values were determined using micrograph analyses on the previously examined samples. Here, the porosity was determined directly using a cut parallel to the build direction of the components as well as perpendicular to it, and then the respective density was calculated according to Equation II.

This procedure was carried out uniformly and consistently for all samples. The results of the individual measurements and component samples are listed in Table 7. For the FDM and LCM processes, the green and sintered components were examined. For the SLS and EBM processes, the as-built components were considered.

4.1.1. FDM

All three designs could be printed as green parts from 316L filament using FDM (Figure 6A-C). The component quality of the cuboid and the cylinder is good, with no visible irregularities or defects. In the femoral head, isolated over-extrusions and defects are visible, which can be attributed to the greater complexity of the component. Due to the curved outer contour and the changing wall thickness of the femoral head, the optimum amount of material was not applied in places. The individual print layers are clearly recognizable on all green parts, leading to a rough component surface, especially on the side walls or curved surfaces.

The sintered components made of 316L are also of good quality, without directly visible defects but with slight localized deformations (Figure 6D-F). The individual print layers are still clearly visible and the surface quality is rough. The components have shrunk considerably as a result of the debinding and sintering process, as the plastic content has been removed from the component and the remaining metal particles have sintered together due to the heat treatment.

(A) Green parts

The pore size in the FDM process typically varies between a few and several hundred micrometers. This means that the corresponding pores can be measured using a gas pycnometer, gravimetric density measurement according to Archimedes, and micrograph analysis. Furthermore, the formation of open and closed pores can occur, which can only be detected to a limited extent depending on the density or porosity measurement method. Especially when 3D-printing green parts from 316L metal filament, the pore size is also similar to that of pure plastic filaments. The measured density values and the resulting porosities of all measurement methods for the FDM-printed green parts made of 316L are listed in Figure 7. The measurement accuracies of the individual measurement methods are listed and considered separately in Section 4.2 in Figure 8.

Gas pycnometry can be used to determine nearly the true density and total porosity of printed green parts very accurately. The helium can penetrate very well into even the smallest open pores deep in the component and displace the air trapped there (closed pores are not reached and are not considered in the measurement). This allows the material density to be measured very accurately. In the samples tested, the theoretical reference density of the filament of 5.00 g/cm³ was always almost achieved. The maximum deviation from this reference was only 0.023 g/cm³ or 0.46%. This also resulted in relatively low porosity values with the maximum of 0.47%. The apparent part density (including the open pores) was therefore not determined here. The influence of the different component geometries on the measurement results was also very low (0.03 g/cm³ or 0.60%) and negligible.

With gravimetric density measurement according to Archimedes' principle, the capillary effect and the surface tension of the measuring medium make wetting and infiltration of the component samples and open pores more difficult, which means that the air is not displaced from the pores and leads to buoyancy, which in turn influences the density.[37] In addition, air bubbles adhere to the components due to surface

Table 7. Average measurement results for part density and porosity of the individual density measurement methods and component geometries

Method	State	Geometry	Cut (to build direction)	Gas pycnometry		Archimedes method		Micrograph analysis	
				Density (g/cm3)	Porosity (%)	Density (g/cm3)	Porosity (%)	Density (g/cm3)	Porosity (%)
FDM	Green	Cuboid	∥	4.9867	0.0849	4.5766	8.4687	4.8743	2.5148
			⊥					4.7908	4.1844
		Cylinder	∥	4.9767	0.4653	4.5811	8.3780	4.8958	2.0842
			⊥					4.8118	3.7644
		Femoral head	∥	5.0078	-0.1560	4.5870	8.2593	4.8264	3.4726
			⊥					4.8244	3.5130
	Sintered	Cuboid	∥	7.8000	2.5000	7.8131	2.3367	7.8485	1.8938
			⊥					7.9578	0.5270
		Cylinder	∥	7.7975	2.5308	7.6730	4.0871	7.8211	2.2364
			⊥					7.8260	2.1752
		Femoral head	∥	7.8110	2.3629	7.7545	3.0683	7.8968	1.2904
			⊥					7.9118	1.1024
SLS	As-built	Cuboid	∥	1.0475	1.6432	0.9431	11.4491	1.0527	1.1514
			⊥					1.0334	2.9630
		Cylinder	∥	1.0454	1.8435	0.9431	11.4460	1.0547	0.9706
			⊥					1.0505	1.3650
		Femoral head	∥	1.0459	1.7934	0.9483	9.5117	1.0005	6.0590
			⊥					1.0287	3.4106
EBM	As-built	Cuboid	∥	4.4249	0.1827	4.4221	0.2451	4.4279	0.1152
			⊥					4.4280	0.1136
		Cylinder	∥	4.4242	0.1985	4.4197	0.2993	4.4289	0.0812
			⊥					4.4259	0.1580
		Femoral head	∥	4.4222	0.2436	4.4103	0.5128	4.4262	0.1536
			⊥					4.4284	0.1040
LCM	Green	Cuboid	∥	3.7035	0.5505	3.5748	4.0064	3.7240	0.0000
			⊥					3.7240	0.0000
		Cylinder	∥	3.7155	0.2282	3.5975	3.3969	3.7240	0.0002
			⊥					3.7240	0.0000
		Femoral head	∥	3.6018	3.2823	3.5358	5.0546	3.7240	0.0000
			⊥					3.7240	0.0002
	Sintered	Cuboid	∥	6.1285	-0.6658	6.0246	1.0414	5.9852	1.6878
			⊥					6.0655	0.3700
		Cylinder	∥	6.0611	0.4419	6.0243	1.0469	6.0799	0.1328
			⊥					6.0723	0.2572
		Femoral head	∥	6.1923	-1.7138	6.0439	0.7244	6.0636	0.4006
			⊥					6.0370	0.8374

Note: Each value is based on three, or in the case of micrograph analyses on five, individual measurements of the respective examined component. The only exception is the density value of the SLS-manufactured femoral head calculated from two measured values, as an obvious outlier value could not be considered. Negative porosities are calculated values and result from the fact that the measured density values are higher in individual cases than the reference values taken from the literature. Statistical analyses of the measured values can be found in Section 4.2, Figure 8.

Abbreviations: EBM: Electron beam melting; FDM: Fused deposition modeling; LCM: Lithography-based ceramic manufacturing; SLS: Selective laser sintering.

roughness and adhesion force, which also cause buoyancy and influence the measured values.[38] The density values determined using Archimedes' method thus characterize the apparent part density (*i.e.*, include the open pores in the measurement) and are therefore lower than the gas pycnometer values. With 0.423 g/cm³ which is equivalent to 8.46%, the deviation from the theoretic reference density is over 18 times higher here than with gas pycnometry. At the same time, the resulting porosities are also significantly higher at approximately 8.2 – 8.5%. For technical applications, however, this is usually the more important value for characterizing the stability of a component. Finally, comparable measured values have also been determined previously[39] using the Archimedes method. The different component geometries have no influence here either (max. 0.22% difference in density).

The total porosity results of the micrograph analyses are between 2.08% and 3.47% for sections parallel to the building direction (∥) and between 3.51% and 4.18% for sections perpendicular to the building direction (⊥) and thus between the results of the gas pycnometer measurement and Archimedes' method. From this, true part densities of 4.83 – 4.90 g/cm³ can be derived from the sections parallel to the build direction and 4.79 – 4.82 g/cm³ perpendicular to it. A small difference can therefore be seen within the micrograph analysis results. Sections parallel to the build direction have a higher density than perpendicular sections. According to Caminero *et al.*,[40] this can be explained by the orientation of the filament strands. Sections parallel to the build direction cut the resulting filament strands horizontally, whereby a relatively large amount of material and fewer pores are always visible under the microscope. Vertical sections, on the other hand, cut these filament strands across the entire cross-section of the component, which means that more pores are visible and therefore the porosity values are higher (Figure 9B). It is not easy to differentiate between filament matrix and pores, which means that measurement inaccuracies also have a major influence with this measurement method (Figure 9, above). In addition, the porosity strongly depends on the respective examined section plane and the measuring fields under consideration and is therefore not representative of the entire component, as completely different values can be present just a few millimeters from the plane in which the cut was being made. Overall, the values determined in this study are within the range reported in the literature (Pellegrini *et al.*[31] and O'Connor *et al.*[32]) or only slightly higher. Ultimately, micrograph analysis is the only measuring method that can optically visualize the actual porosity with open and closed pores (at least in the area under consideration). However, the component geometry cannot be meaningfully characterized here, as the geometry is not depicted in the 2D section examined. Micrograph analyses can also be used to assess the size and morphology of the pores, which allows the harmfulness of the pores to be estimated. Large and irregular pores are generally more harmful than small and spherical pores.

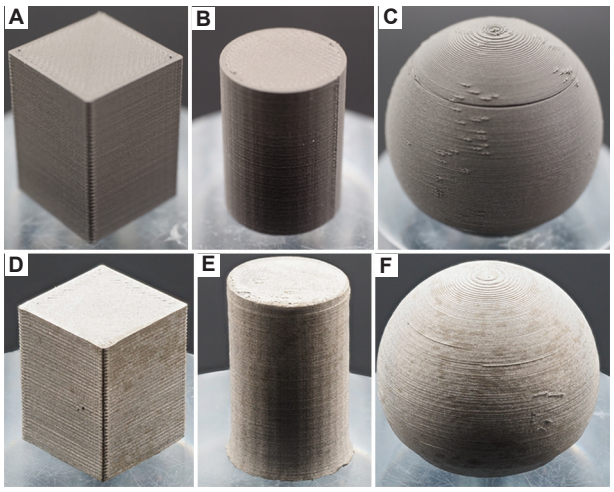

Figure 6. FDM-printed 316L parts. (A-C) Green parts directly after printing; (D-F) 316L stainless steel sintered metal parts
Abbreviation: FDM: Fused deposition modeling

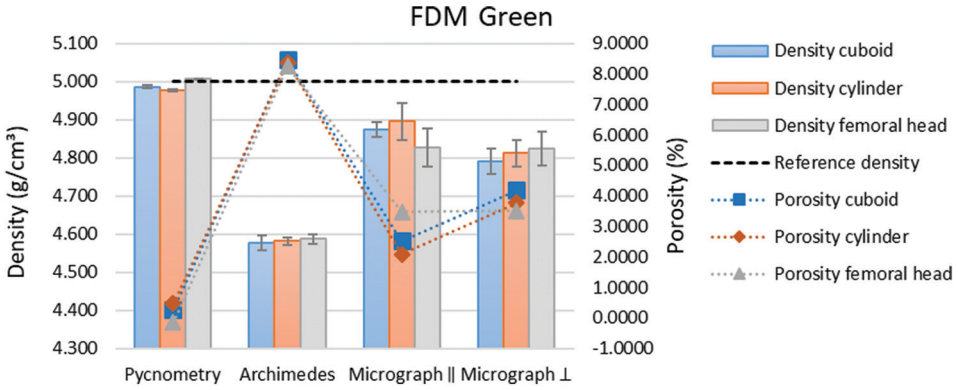

Figure 7. Measured density and porosity values of additively manufactured stainless steel green parts

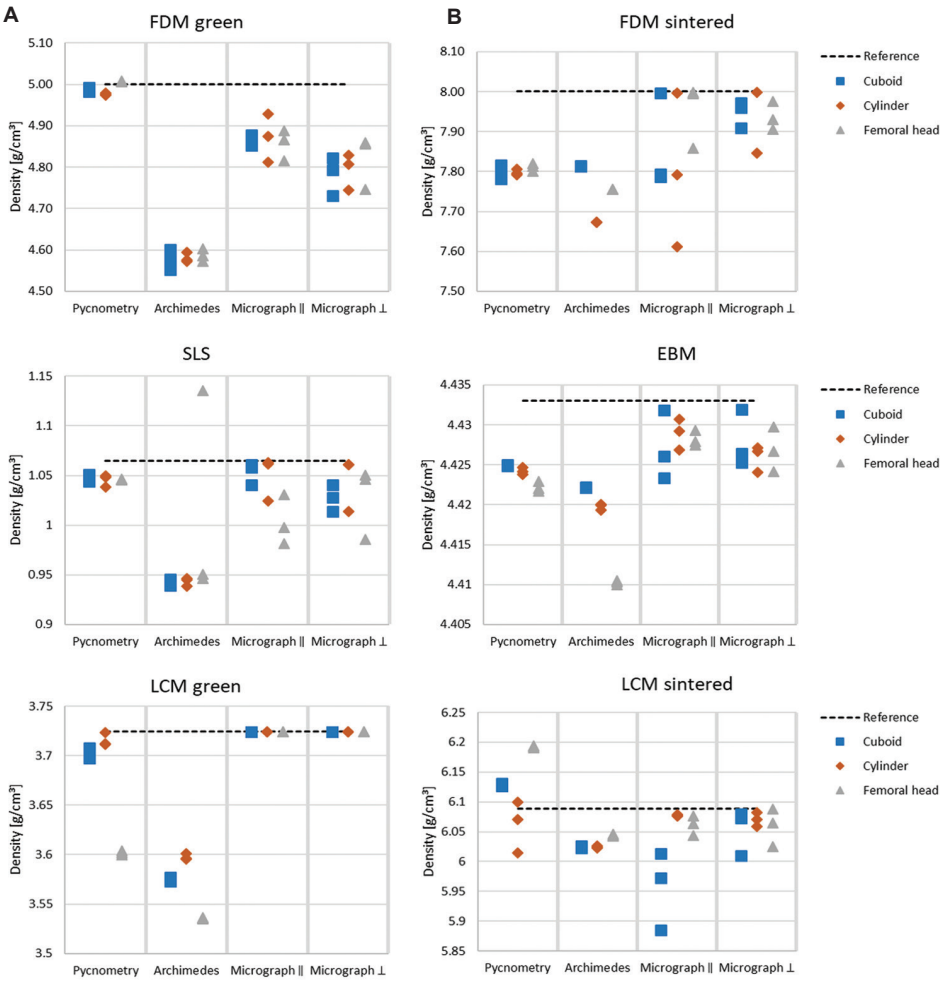

Figure 8. Comparison of the variance and range of the analyzed density measurement methods for the individual additive printing processes
Abbreviations: EBM: Electron beam melting; FDM: Fused deposition modeling; LCM: Lithography-based ceramic manufacturing; SLS: Selective laser sintering

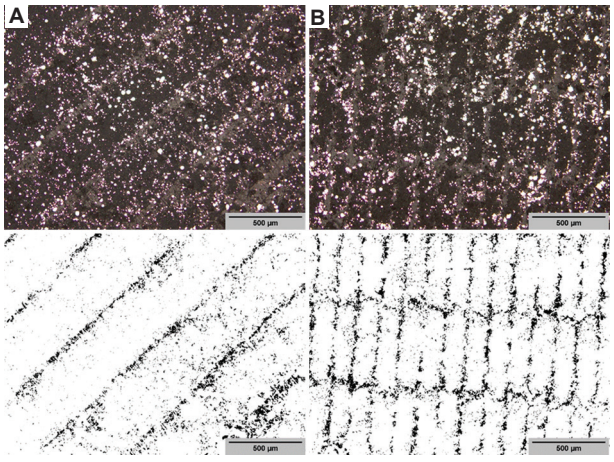

Figure 9. Micrographs (top) and binary images created using ImageJ (bottom) for micrograph analyses of FDM green parts made of 316L. (A) Section parallel to the build direction; (B) section perpendicular to the build direction. Scale bar: 500 µm
Abbreviation: FDM: Fused deposition modeling.

(B) Sintered parts

Sintered components made from 316L metal filament have a different pore size and pore structure than the printed 316L green parts. The basic 316L filament consists of a mixture of polymer binders and metal particles and is only converted into a dense metal part after the printing process through debinding and sintering processes. The pores change in the various process phases from the green part to the sintered component. After debinding, the polymer components are largely removed, creating additional open pores in the green part. During sintering, the metal particles combine and sinter to form a dense component. Due to incomplete fusion of the metal particles during sintering, open and closed pores continue to occur. The pore size is usually smaller than the initial pore size of the green parts after printing, but can still be in the range of a few micrometers. This means that the samples can also be easily analyzed with the measurement methods

used. The measured density values and the determined porosities of all measurement methods for the sintered FDM components made of 316L are listed in Figure 10 (accuracies of the measurement methods in Figure 8).

Gas pycnometry can be used to determine the density and porosity values of sintered 316L metal parts with repeatable accuracy. The helium used can penetrate the open pores in the component, which are greatly reduced and minimized by the sintering process, and displace the air there. Closed pores and pores further inwards cannot be reached due to the higher component density. In principle, only apparent density values can be measured with the gas pycnometer for the sintered 316L samples, but these represent almost the true density. This becomes clear from the deviation from the theoretical reference density value, which is 8.00 g/cm³. The values determined using gas pycnometry deviate from this by 0.20 g/cm³ or 2.50% and result in an open porosity for the components of 2.36 – 2.53%. This is slightly higher than the values determined in the literature by Gong *et al.*[24] However, the differences are small and may be attributed to the printing parameters, component geometries, measuring devices, or measurement settings used, whereas the component geometry only has minimal influence on the measurement results.

With gravimetric density measurement according to the Archimedes' principle, capillary effects occur again, which have a negative impact on repeatability. Closed pores and smaller open pores are not infiltrated by the measured medium. In addition, the dense, sintered metal samples have less air in the component overall, which means that the influence of porosity is less pronounced and the measured values are comparable to those of gas pycnometry. The deviations from the reference density here are max. 0.33 g/cm³, which corresponds to 4.13% and is almost near to the range of the gas pycnometer values. This results in open porosity values of 2.34 – 4.09%, which is higher than the literature values in some cases. The deviations and fluctuations probably result from the component geometry in combination with the debinding and sintering process. In the literature, Gong *et al.*[24] and Caminerio *et al.*[40] printed relatively flat components with low wall thicknesses, whereas components with comparatively large wall thicknesses were produced in this work. With thicker walls, however, the debinding and sintering process takes longer time, and more polymer is burnt out of the component, resulting in more pores and higher porosity.[31] In addition, the process-related pores between the filament strands remain in the components even after sintering (Figure 11), whereas air and gases collect in these pores, which in turn cause buoyancy in the gravimetric density measurement and reduce the part density as compared that reported in the literature. This is more noticeable in the results with greater wall thicknesses than with thinner ones, which explains the deviations from the literature. Due to the different component geometries and wall thicknesses, the material feed (extrusion width) also changes locally, and the debinding liquid and the heat during sintering also affect the components differently, which has an influence on the density and which in particular explains the fluctuations in the density values.[41,42] This suggests a geometry dependence of the density measurement values, which can also be depicted somewhat here with a maximum density deviation of 1.79%. However, it cannot be clearly demonstrated which geometric factor was decisive for this deviation.

In the micrograph analysis, total porosities of 1.29 – 2.24% parallel and 0.53 – 2.18% perpendicular to the build direction were determined. This results in a calculated true part density of 7.82 – 7.90 g/cm³ (∥) and 7.83 – 7.96 g/cm³ (⊥). Parallel sections here show a slightly lower but almost equal part density than perpendicular sections, which in turn can be explained by the shrinkage of the parts, which closes the space between the layers. Overall, the micrograph values are slightly higher than those of gas pycnometry and the

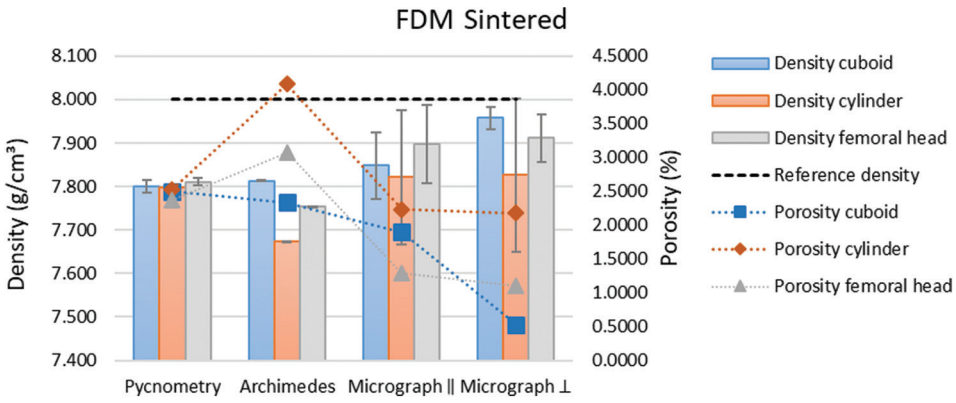

Figure 10. Measured density and porosity values of additively manufactured and sintered stainless steel parts
Abbreviation: FDM: Fused deposition modeling

Archimedes method. The deviations can be explained by the fact that in the micrograph analysis the pores actually present, including the closed pores, are included in the (true) density determination. With the other two methods, the closed pores are not included in the (apparent) density calculation. In addition, subjective optical settings in the evaluation software such as brightness, resolution, and visualization influence the measurement results when determining the porosity of the micrograph analysis, which leads to deviations. It should also be noted that the micrograph analysis only provides an insight into the microstructure of the components at the component plane under consideration and is not representative of the entire component. For example, the area under consideration may have a higher density, but the rest of the component may have a lower density. A geometry dependency can also be recognized here, which is similar to the Archimedes method. However, this does not serve as proof of a geometry dependency, as the geometry is not mapped here in the analysis of a 2D grinding plane.

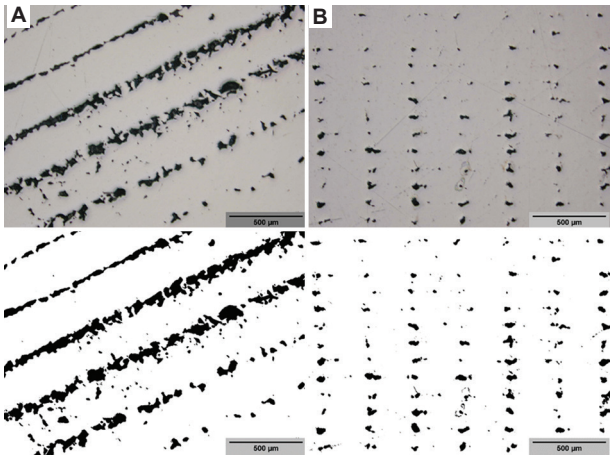

Figure 11. Micrographs and binary images for micrograph analyses of sintered FDM components made of 316L. (A) Section parallel to the build direction; (B) section perpendicular to the build direction. Scale bar: 500 µm
Abbreviation: FDM: Fused deposition modeling

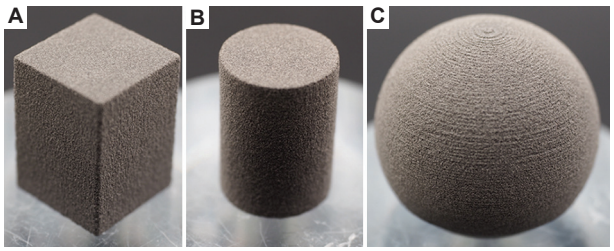

Figure 12. Laser-sintered PA12 components. (A) Cuboid; (B) cylinder; (C) femoral head

4.1.2. SLS

Using SLS, all three component designs were successfully manufactured in one printing process (Figure 12A-C). All components are of good quality with no visible defects or irregularities. The individual print layers are not or are only very slightly recognizable. However, the component surface is very rough. Sharp edges are less detailed and rounded on all components, as the size of the individual powder particles has a limiting effect on the sharpness of the edges.

The pore size in SLS-generated components depends on the process parameters and material properties used but is in the range of 1–50 µm for PA12 powder. Gas pycnometer and the Archimedes buoyancy method are therefore very suitable for measuring pores in this size range, since micrograph analyses may not be able to capture smaller pores well. In SLS-generated components, there are open and closed pores, with the latter filled with air, gases, or even unfused powder. The density and porosity values determined for the SLS components for all measurement methods are listed in Figure 13 and the accuracies of the respective measurement methods are displayed in Figure 8.

The density of the PA12 plastic components measured by gas pycnometer is almost a true and reproducible density for all test components. The helium molecules can easily penetrate the component through the smallest open pores

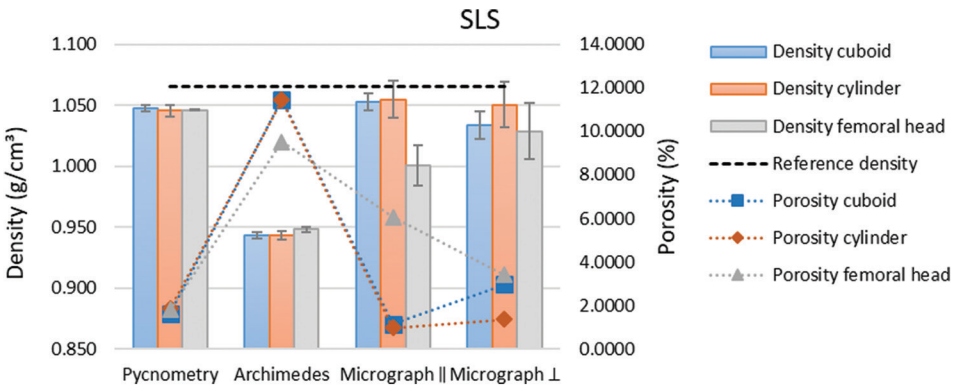

Figure 13. Measured density and porosity values of additively manufactured SLS PA12 parts

and displace the air. This makes it possible to determine the material density of the component, which is 1.065 g/cm³ for the PA12 powder. The gas pycnometry of the PA12 samples thus results in only 0.02 g/cm³ which is equivalent to 1.88% deviation from this reference, which leads to total part porosities of 1.64 – 1.84% due to the comparatively loose sintering of the powder particles. The values are lower than the values collected in the literature,[22] but these results can only serve as a reference to a limited extent, as the powder used, printing system and process parameters differ, but these have a major influence on the resulting part porosity. However, a slight difference in density between the unprocessed reference powder and the sintered powder is understandable, as the density depends on the degree of crystallinity and the unprocessed PA12 powder has a higher degree of crystallinity (and thus a higher density) than the sintered, melt-crystallized PA12.[22] An influence of the component geometry cannot be determined.

Using the Archimedes method, only apparent densities were measured and open porosities were determined, as the measuring liquid could not penetrate well into the small open pores. In addition, air bubbles easily collect on the rough sample surfaces and due to capillary effects, causing additional buoyancy of the samples. This also slightly influences the measured density values. Compared to the gas pycnometry, the density values determined using Archimedes method deviate significantly more from the reference geometry with 0.12 g/cm³ or 11.23%. The deviation is therefore almost 6 times higher than the gas pycnometer values and is also reflected in the porosity values of 9.51 – 11.45%. The density values are very similar for all component geometries. A general geometry dependency therefore cannot be determined.

The micrograph analysis provides total porosities of 0.97 – 6.06% parallel and 1.37 – 3.41% perpendicular to the build direction. This results in part densities comparable to 1.00 – 1.06 g/cm³ (∥) and 1.03 – 1.05 g/cm³ (⊥). The micrograph analysis considers both open and closed pores and confirms the gas pycnometer measurements in principle. This results in differences in density and porosity between the sections of the two build directions, which, however, do not show a uniform pattern and can therefore be attributed to the conditions in the respective section plane under consideration (Figure 14). The component geometry may have an influence here, as the femoral head in particular has a significantly lower density. However, the density values also differ significantly between the cutting directions, so the influence of the component areas under consideration probably has a greater impact.

4.1.3. EBM

With EBM, all component designs could be produced in one printing process (Figure 15A-C). The component

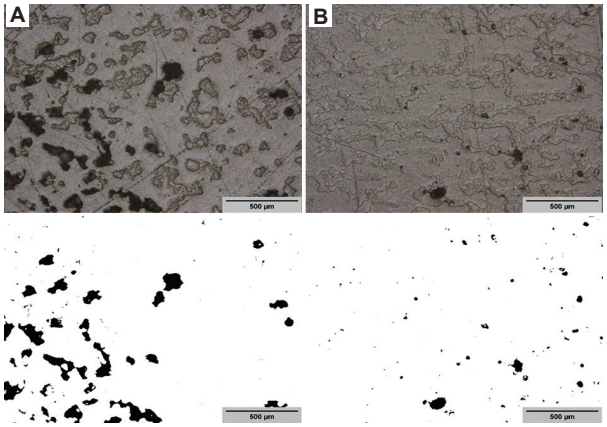

Figure 14. Micrographs and binary images of SLS components made of PA12. (A) Section parallel to the build direction; (B) section perpendicular to the build direction. Scale bar: 500 µm
Abbreviation: SLS: Selective laser sintering

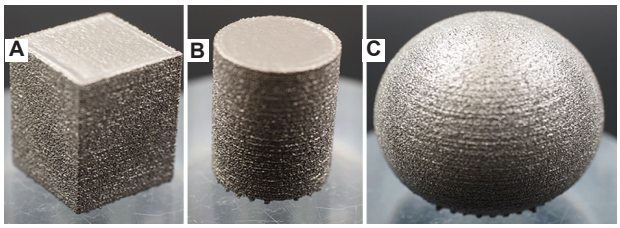

Figure 15. (A-C) Additively manufactured EBM components made of Ti6Al4V
Abbreviation: EBM: Electron beam melting

quality is always comparable, without defects and irregularities. However, all components have remnants of support structures on one side that could not be completely removed by hand. Individual component layers were recognizable on all components. The components were also very rough. Only the component surface of the cuboid and the cylinder had a significantly smoother surface, as the electron beam was able to fuse these areas together very well without adhering loose powder particles.

The size of pores in EBM components is usually <100 µm, although these can also be significantly smaller than 50 µm due to carefully selected process parameters. Gas pycnometry, gravimetry, and micrograph analysis can detect these pores well. Similar to the powder-based SLS process, both open and closed pores occur in EBM. The formation process is similar to SLS and usually results from trapped gases, incomplete melting of the powder, and unfavorable process settings. The part densities and porosities of the individual EBM test components determined using the measurement methods used are shown in Figure 16. The measurement accuracies of the three measurement methods are listed in Figure 8.

The measured gas pycnometer density of the EBM test components of max. 0.01 g/cm³ or 0.23% is slightly

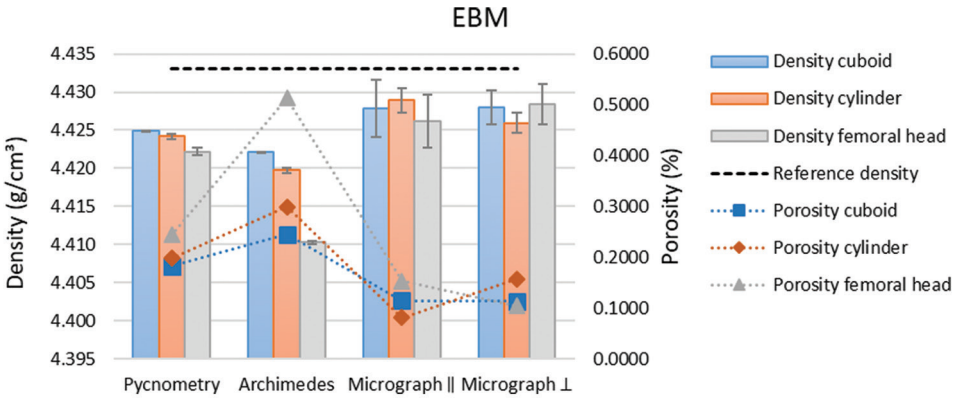

Figure 16. Micrograph analysis for porosity measurement of an additively manufactured titanium part

lower than the measured bulk density of titanium of 4.433 g/cm³. The porosity is also only 0.18 – 0.24%. In this case, an apparent density is theoretically measured here. In practice, the deviations from the reference density are very small, so a true density can be assumed. Small deviations are understandable, as the EBM samples are densely fused together and generally have very few pores (Figure 17). As a result, the helium can only reach the surface of open pores in the EBM samples and cannot reach closed pores at all, displacing the air or gas contained therein. This results in slight measurement deviations from the material density as the reference value. Furthermore, light elements in the powder can also be vaporized during the EBM process, which changes the chemical composition of the titanium and therefore the measured part density.[38] A slight dependence on geometry is recognizable, but this is also very slight in absolute terms.

The Archimedes density of the EBM samples is max. 0.02 g/cm³ or 0.45% lower than the reference geometry and results in 0.25 – 0.51% open porosity. This means that the apparent density results of the Archimedes method, in this case, deviate only slightly (max. 0.22%) from the results of gas pycnometry. With other AM methods, especially PBF such as SLS, the results of these two measurement methods differ significantly more. One reason for this is the lower porosity. The dense EBM components do not absorb any measuring fluid with the Archimedes method and absorb almost no gas with gas pycnometry. This means that internal pores are not infiltrated and are included in the calculation of the apparent density for both measurement methods. However, small accumulations of air on the rough component surface can still slightly reduce the density with the Archimedes method and lead to small fluctuations. These effects are geometry-dependent and are particularly noticeable in the femoral head, which has a larger component surface and a bore.

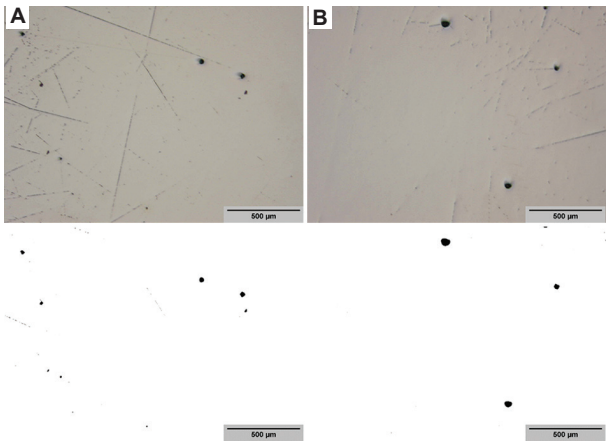

Figure 17. EBM micrographs and binary images. (A) Section parallel to the build direction; (B) section perpendicular to the build direction. Scale bar: 500 µm
Abbreviation: EBM: Electron beam melting

The total porosities determined by micrograph analysis are approximately 0.08 – 0.15% (‖) and 0.10 – 0.16% (⊥). This results in true density values of approximately 4.426 – 4.429 g/cm³ for a cut parallel and 4.426 – 4.428 g/cm³ for a cut perpendicular to the build direction. The micrographs are shown in Figure 17. As a result, all the measurement methods analyzed (gas pycnometry, Archimedes method, and micrograph analysis) achieve similar values for the EBM test components. The maximum deviation between all individual measurements is only 0.02 g/cm³ or 0.45%. This confirms Delesse's principle, which states that the ratio of the area occupied by a component to the total profile area is a consistent estimate of the volume fraction of the component in the object.[43] Terris *et al.*[38] were also able to prove this. However, micrograph analysis tends to slightly underestimate the porosity values and overestimate the density values compared to both other methods. One explanation for this could lie in the morphology of the porosity, which is mainly random and irregular in AM.[38]

Another explanation could be that the porosity rate at the sample surface or near the surface is generally higher, which is almost not considered in the micrograph analysis.[38] A special geometry-dependent influence may exist but cannot be explained comprehensibly with the micrograph analysis, as the component areas under consideration do not include the component geometry.

4.1.4. LCM

In the LCM process, the various component designs were produced individually in three different print jobs (Figure 18A-C). The same batch of material was always used. The resulting part quality of all components was ultimately comparable, without defects or cracks. However, the surface quality of the cuboid and the cylinder is occasionally characterized by superficial material adhesions. These irregularities did not occur with the ball head. However, it was necessary to print with a raft so that the components adhered to the building platform. This raft then had to be removed manually, which was not possible without leaving any residue.

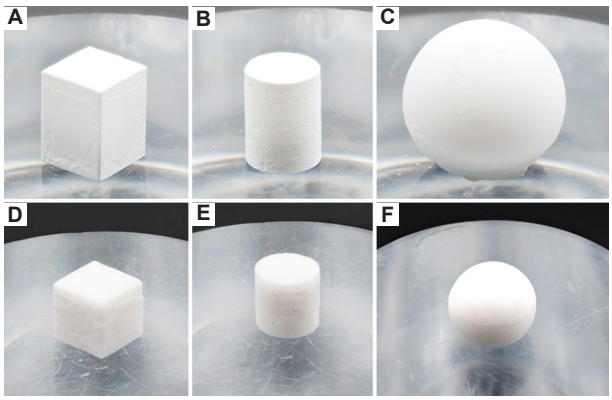

Figure 18. Ceramic parts printed with zirconium oxide and LCM process. (A-C) Green parts directly after printing; (D-F) sintered ceramic parts
Abbreviation: LCM: Lithography-based ceramic manufacturing

Individual component layers are not recognizable in any of the designs.

The sintered ceramic components have an uneven surface quality (Figure 18D-F). Areas with material adhesions and small cracks are clearly recognizable, but there are also good areas without irregularities, which are relatively smooth. The components have also shrunk considerably as a result of the sintering process and the burning out of the plastic content.

(A) Green parts

The pore size of zirconium oxide green parts printed using the LCM process is typically less than 50 µm. In principle, open and closed pores can occur, but the number of pores in the green parts is minimal in this process and closed pores predominate. The measured density values and the resulting porosities of all measurement methods for the LCM green parts made of zirconium oxide are listed in Figure 19 (accuracies of the measurement methods are displayed in Figure 8).

Using the gas pycnometer, nearly true densities were measured for the ceramic green parts made of zirconium oxide. These density values correspond approximately to the reference density of 3.72 g/cm³ determined for an LCM-printed green part with the same printing parameters and the same material batch. The maximum deviation is 0.12 g/cm³ equivalent to 3.22% and lead to porosity values of 0.23 – 3.28%, which are caused by the few open pores that are present as a result of the printing or cleaning process of the green parts. A slight dependence on geometry can be recognized (maximum deviation of 0.11 g/cm³ which is equivalent to 2.96%). It can be seen that the simpler the component geometry and the smaller the resulting component surface, the higher the density.

The same situation results from the Archimedes measurements with an apparent density. From this,

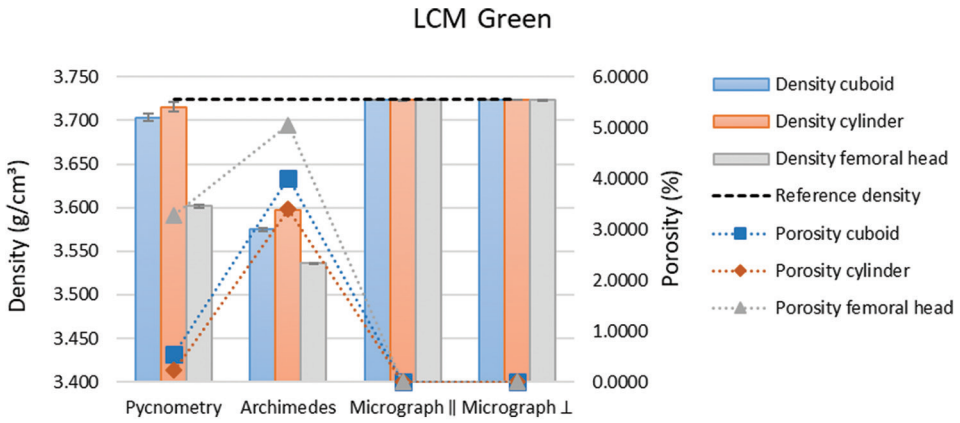

Figure 19. Measured density and porosity values of additively manufactured ceramic green parts

deviations of max. 0.19 g/cm³ or 5.10% from the reference density and porosities of 3.40 – 5.06% can be determined. The small deviation of 2.14% from the gas pycnometer measurements is understandable, as the few and very small open pores cannot be measured with the Archimedes method and are therefore not included in the density determination. The apparent part density is determined with a slightly lower density and higher porosity. A geometry dependency can also be recognized here, which is comparable in principle to the situation with gas pycnometry.

The porosity in the green parts was then analyzed optically using micrograph analysis. Very occasional pores were discovered, but these were not significant in relation to the entire field of investigation (Figure 20), as the porosity was 0.00% for all components, both in the sections perpendicular to the build direction and in those parallel to the build direction. This was then used to calculate a part density of exactly 3.72 g/cm³. For the LCM green parts, micrograph analysis is therefore theoretically the most accurate measurement method for determining part density and porosity. Gas pycnometry and Archimedes' method provide comparable, but usually slightly lower density values. However, it should again be noted that only a specific area is considered here and not the entire component. The component geometry is therefore not considered here.

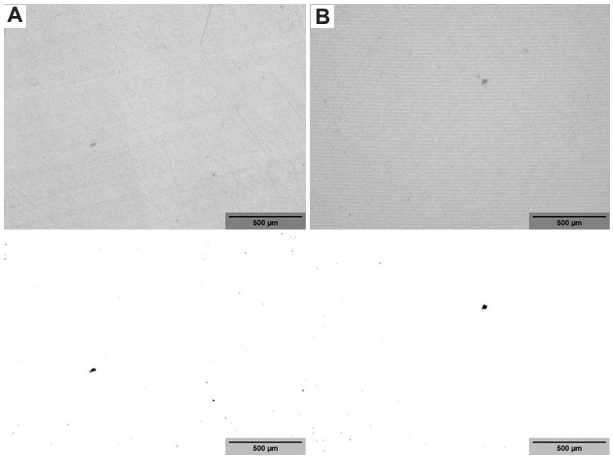

Figure 20. LCM micrographs and binary images of the green parts made of ZrO_2. (A) Section parallel to the build direction; (B) section perpendicular to the build direction. Scale bar: 500 µm
Abbreviation: LCM: Lithography-based ceramic manufacturing

(B) Sintered parts

By sintering the LCM green compacts, the pore size is further reduced and is then in the range of 0.1 – 5 µm. Of the methods investigated in this work, only gas pycnometry and buoyancy measurement are suitable for taking the pores into account with sufficient accuracy in the measurements. Micrograph analyses may be less accurate for such small pore sizes. The sintering process typically causes the pore structures to change somewhat. Open pores close and closed pores become smaller, as individual print layers also fuse and the component shrinks. The measured density values and the determined porosities of all measurement methods for the sintered LCM ceramic components made of ZrO_2 are listed in Figure 21. The accuracies of the measurement methods are analyzed in more detail in Figure 8.

Using the gas pycnometer, true density values were measured for all components in the sintered ZrO_2 samples. Compared to the reference density of 6.088 g/cm³ for the AM and sintered ZrO_2, the maximum deviation is 0.10 g/cm³ or 1.64%. However, two of the density values determined are higher than the reference density. Nevertheless, these values are within the range of the literature values,[30,36] but in some publications the comparative values are also significantly lower.[28,29] The resulting open porosities for the components

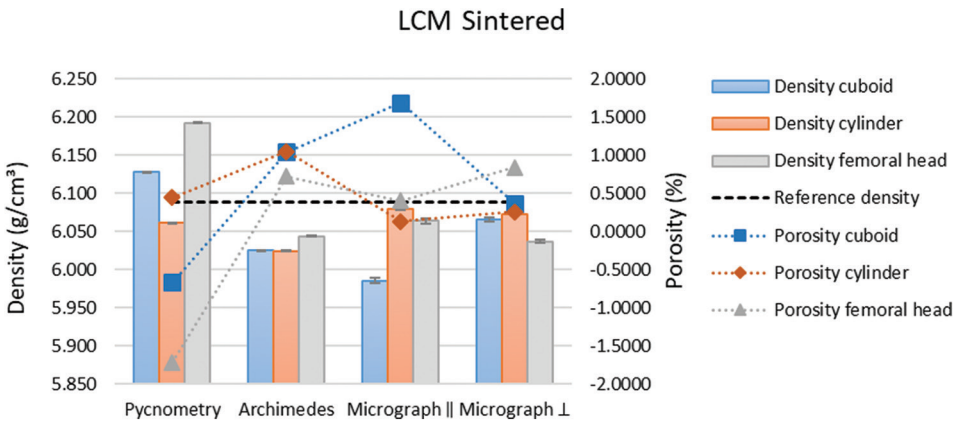

Figure 21. Measured density and porosity values of additively manufactured and sintered ZrO_2 parts

are of -1.71% to 0.44%, which is significantly lower than those determined by Llanos,[29] for example. However, the measured values are difficult to compare, as Llanos[29] used a micrograph analysis and therefore only measured in one sectional plane. Negative porosity is also not possible and results mathematically from the fact that some of the determined densities are higher than the reference density of 6.088 g/cm³ determined by the material manufacturer. The deviations between the density values are relatively small and can occur, for example, due to the use of different measurement methods. According to the material manufacturer, the reference density of the sintered sample was determined by means of buoyancy measurement according to Archimedes method, which generally leads to slightly lower density values than with gas pycnometer measurements. If one looks at the microscopic images of the analyzed samples (Figure 22), one can also clearly see the presence of pores, which lead to porosities of more than 0%. The gas pycnometer was therefore used to measure the true density of the sintered ZrO_2 components, which is slightly higher than the reference density measured according to Archimedes method or the density determined in the literature using this measurement method. The measurement results also show a geometry dependency. However, this is relatively low in absolute terms, probably attributed to the sintering process. Nevertheless, it can also be seen that the more complex the component geometry and the larger the resulting component surface, the higher the density – in other words, the opposite behavior to that of the green parts made of ZrO_2. It can therefore be assumed that a larger component surface area leads to a better sintering process and a higher density.

Measurements using the Archimedes method itself on the components analyzed in this study show relatively

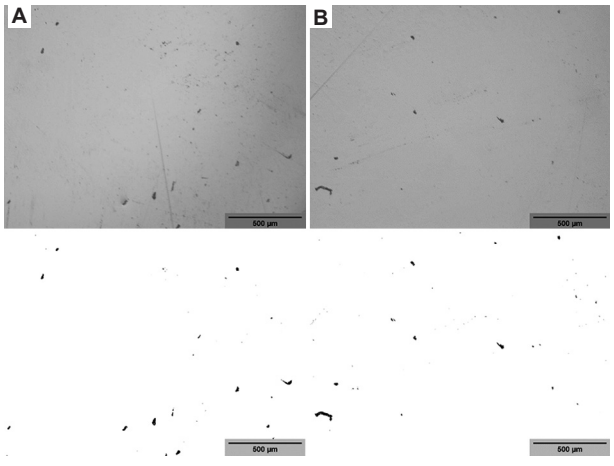

Figure 22. Micrographs and binary images of the LCM ceramic components made of ZrO_2. (A) Section parallel to the build direction; (B) section perpendicular to the build direction. Scale bar: 500 µm
Abbreviation: LCM: Lithography-based ceramic manufacturing

constant apparent part densities. The deviations from the reference density are of maximum 0.06 g/cm³ (0.99%), resulting in open porosity values of 0.72 – 1.05%. The density values determined are therefore always slightly below the reference value from the material manufacturer, but are in good agreement with the other literature.[28-30] Deviations from the reference value can occur, for example, due to different printing or cleaning settings, but are generally low. This also applies to deviations between the analyzed component geometries, which are marginal here.

Total porosity values of 0.13 – 1.69% (∥) and 0.26 – 0.84% (⊥) were determined by micrograph analyses, which lead back to true part densities of 5.99 – 6.08 g/cm³ (∥) and 6.04–6.07 g/cm³ (⊥). This validates the reference and buoyancy measurements very well and also agrees with the results of Llanos[29] and Suominen *et al.*[30] The values determined with the gas pycnometer are slightly higher than the values determined by analyzing the micrograph, but also take the entire component into account. During the micrograph analyses, it was noticed that there were isolated cracks inside the components. Crack formation is a known problem when sintering powder components and is caused by residual stresses that counteract component shrinkage.[44] The cracks can sometimes affect the optical determination of porosity and falsify individual measurements, leading to higher porosities or lower apparent densities. This can also contribute to the small differences between apparent and true density or between reference, buoyancy, and micrograph measurements and the gas pycnometer measurements. In the analyses carried out in this work, corresponding cracks were detected twice in the investigated areas and excluded from the porosity calculation in the best possible way on the software side. Influences due to the component geometry are not considered here for procedural reasons.

4.2. Comparison of density and porosity determination methods used

A comparison of the three analyzed density and porosity measurement methods – gas pycnometry, the automated Archimedes method, and micrograph analysis – is initially made on the basis of published literature[6] and newly defined criteria, which are listed in Table 8.

In practice, non-destructive, highly accurate, highly repeatable, and reproducible measurements are usually important. In principle, gas pycnometry and Archimedes' method are non-destructive. In micrograph analysis, smaller samples have to be removed from the components to be analyzed, an action that usually destroys the component. With regard to measurement accuracy, Figure 8 compares the density measurement results of gas pycnometry and the automated Archimedes method

Table 8. Comparison of different aspects of the density and porosity measurement methods

Criteria	Pycnometry	Archimedes method	Micrograph
Non-destructive testing	●	●	○
Geometry dependencies	◪	◪	◪
Measurement effort and costs	◪	◪	◪
Repeatability of measurements	●	◪	○
Complexity of the process	◪	◪	◪
Accuracy of measurements and results	●	◪	◪
Short measuring cycle	◪	●	○
Direct density measurement	●	●	○
Detection of pore morphology	○	○	●
Detection of pore distribution	○	○	●
Ability to measure the true density	◪	◪	●
Ability to measure the apparent density	◪	●	○

Note: ●: Denotes yes, good, low; ○: denotes no, bad, high. The symbols between the black full circle and the white full circle are gradations of the respective designation. There is no direct description for this, it is more like visualizations that the criterion is closer to yes, etc. or no, etc.

as well as the density values calculated by micrograph analysis for the individual components. The individual diagrams clearly show the individual density values and the reference density for each measurement method and also roughly visualize the resulting range, the variance, and the deviation from the respective reference value.

The diagrams show that the gas pycnometry often exhibits a low variance and range in the individual measurements among each other as well as between the measurements of the respective component geometries and usually deviates only slightly from the reference values. The gas molecules of the helium gas used are not prevented from penetrating the pores by capillary effects or surface tensions and can therefore penetrate even the smallest open pores so that only the closed pores are not reached and are not included in the density calculation. The resulting density values often almost characterize the material density of the material used or come closest to it of all the measurement methods examined. This method can therefore usually be used to directly measure the true density. However, it should be noted that gas pycnometry can tend to overestimate the density values when the apparent density is actually of interest. Depending on the application or further utilization of the measured values, the true density may not correspond to the real conditions and the component may appear to have better mechanical properties than it actually has.

Compared to gas pycnometry, the density values of the Archimedes method always deviate more strongly from the reference density value and show lower part densities. In addition, the deviation between the component geometries is also higher in some cases. The variance and the range are comparatively small, especially between the individual measurements of a component. Due to capillary effects and the surface tension of the infiltration fluid on the component surfaces, smaller open pores cannot be infiltrated as well with the Archimedes method and are therefore not included in the density calculation in addition to the closed pores. This results in lower density values than those with gas pycnometry. Air bubbles adhering to the component surface in the measuring fluid can also cause additional buoyancy, which falsifies the density calculation. The Archimedes method can therefore be used more for direct measurement of the apparent part density. The density here is lower than the material density, as the enclosed air or porosity is partly considered and reduces the density. This usually corresponds better to the real conditions in the component and is also more advantageous, especially for technical aspects, as the mechanical properties of the component can be predicted more realistically. Gravimetric density measurement according to Archimedes method is also very reliable, accurate, fast, and easy to automate, making it effective for industrial component characterization.

The micrograph analysis shows slightly higher values for the variance and the range of the results compared to the other two measurement methods, but still at a low level overall. Micrograph analysis is the only measurement method investigated that also includes the closed pores in the calculations. However, the porosity is measured first and then calculated back to the density. Furthermore, the values are only meaningful for the area of the component under consideration and are not representative of the entire component. In most cases, they basically confirm the values of gas pycnometry and buoyancy measurement and often lie between the measured values of these two methods.

Since the individual specimens were analyzed several times under identical conditions using the measurement methods examined, the repeatability, *that is*, the ability of the measurement methods to produce consistent results, can be assessed. High repeatability is characterized by low standard deviations in the results of multiple repeated measurements. It can be concluded from standard deviations depicted in Figures 7, 10, 13, 16, 19, and 21 that gas pycnometry and Archimedes' method exhibit very good repeatability, while micrograph analyses are subject to comparatively high fluctuations.

Ultimately, further criteria for selecting one method over the others should also be taken into account. Terris *et al.*[38] recommend determination of method based on the type of sample (shape, size, destructible or not), the desired results (type of density or porosity, position, trend between the samples), the available material, and the time available. The findings of the current study can also be used to derive general statements on the application of density and porosity measurement methods for individual additive process categories listed in Table 1. All AM processes that already produce relatively dense components due to the process can, in principle, be analyzed very precisely using gas pycnometry or the Archimedes method. Due to the low porosity and usually only a few open pores, the measurement results of both methods are comparable. In this case, the true density determined using the gas pycnometer corresponds approximately to the apparent density determined using Archimedes method. This usually applies to the AM processes directed energy deposition, material jetting, metal PBF, sheet lamination, and VPP. AM processes, which tend to produce porous components due to the nature of the process, a distinction should be made between true and apparent density during analysis. The true density should always be determined using gas pycnometer measurements and the apparent density using the Archimedes method. As a rule, the true density will always be somewhat higher and lead to less part porosity than the apparent density values. This must ultimately be considered when characterizing the component to predict the mechanical properties of a component as realistically as possible. This procedure applies to binder jetting, MEX, polymer PBF, and VPP green parts.

The automated form of Archimedean density measurement is generally very well suited to industrial production practice in particular, as it is more economical than the other methods. The measurements are as accurate as with the other measurement methods, but can be carried out much faster and are also more reproducible, less prone to errors, and easy to integrate into industrial process chains thanks to increasing automation. The automated Archimedean process can potentially also be used for the preliminary inspection of green parts in two-stage AM processes to quickly and relatively accurately obtain initial information on part density and porosity, which can then be used to decide whether the green parts can be further processed or directly rejected. This contributes to saving resources and increasing process quality.

5. Conclusion

In this work, gas pycnometry, gravimetric buoyancy measurement according to Archimedes method, and micrograph analysis were analyzed and compared with each other as density measurement methods for AM components. In this regard, the basics of density determination were worked out, and basic density and porosity values were researched from the existing literature. AM processes and designs for the production of test samples were then defined, the printing systems parameterized and the samples manufactured. This was followed by a quality assessment as well as density and porosity determination of the test samples according to defined standard specifications. First, FDM-printed components made of 316L stainless steel filament were analyzed, whereby green parts were first examined after the printing process and then the final components after a sintering process. Furthermore, SLS and EBM components made of PA12 or titanium powder as well as ceramic components that were printed using the LCM process from a zirconium powder-loaded slurry, initially as green parts and after a sintering step also as final ceramic components, were analyzed.

The results of this study supplement and expand the state of the art in terms of component density and porosity of the specimens produced using the AM processes investigated. In addition, the results obtained in the present study can be generalized and recommendations for the measurement of porosity and density can be derived for other AM processes. Detailed measured values are presented, which are also determined and validated using three different measurement methods. Based on a detailed comparison of the resulting density and porosity results between the density measurement methods used and between the results of the individual printing methods, the advantages of the individual measurement methods for certain AM process categories and processing materials were identified. Gas pycnometry is best suited for determining the true density of components and the Archimedes method for determining the apparent density. Gas pycnometry is recommended for all AM processes that already produce relatively dense components due to the process. The Archimedes method is advantageous for AM processes that tend to produce porous components. For these parts, a distinction must be made between true

and apparent density. The apparent density reflects the real conditions in the component more realistically and is more suitable for analyzing the component's mechanical properties. Thanks to the increasing automation of the Archimedes method, the apparent part densities can also be determined in the most repeatable and reproducible way possible. Therefore, gas pycnometry and the automated Archimedes method are the two high-precision density measurement methods, which differ from each other in economic aspects. The Archimedes method is more favorable for industrial applications because it is easier to automate. Automated handling of test specimens can also achieve a significant increase in accuracy and reproducibility as well as cost-effectiveness compared to manual measurements according to Archimedes method. The method is therefore also suitable for integration into industrial process chains and for fast and cost-effective preliminary testing of green parts in two-stage AM processes to obtain initial information on part density and porosity quickly and relatively accurately. This information can then be used to decide whether the green parts can be further processed or directly rejected. This contributes to saving resources and increasing process quality.

In future work, the results obtained in this study should be supplemented by analyzing other AM process categories. Furthermore, CT analysis should be included in the investigations as an additional measurement method that is very relevant in the AM sector. It is also recommended that the aspect of preliminary testing of green parts be pursued further. For example, reference values for green parts could be determined using gas pycnometry and validated using automated Archimedean density measurements and CT analyses. The automated Archimedes method should be successively optimized so that it enables high accuracy and offers stable, fast, and economical measurement, especially for green parts. This ultimately increases process quality and can contribute to more sustainable AM.

Acknowledgments

The authors gratefully acknowledge the Dimensionics GmbH for their technical support and for performing the automated density measurements according to the Archimedes principle.

Funding

This research was funded by the European Union, which was made available through the European Regional Development Fund (ERDF) and the Ministry for Economics, Employment and Health of Mecklenburg-Vorpommern (grant numbers TBI-V-1-396-VBW-136 and TBI-1-026-W-009).

Conflicts of interest

Dimensionics GmbH is the manufacturer of the automatic density measurement system "Density L" and a project partner in a research project with the University of Rostock. Dimensionics GmbH had no role in study design, data analysis, decision to publish, or preparation of the manuscript. The authors listed are not associated with the Dimensionics GmbH.

Authors' contributions

Conceptualization: Erik Westphal
Data curation: Erik Westphal
Formal analysis: Erik Westphal
Funding acquisition: Erik Westphal, Hermann Seitz
Investigation: Erik Westphal, Hermann Seitz
Methodology: Erik Westphal
Resources: Erik Westphal
Software: Erik Westphal
Supervision: Hermann Seitz
Validation: Erik Westphal
Visualization: Erik Westphal
Writing – original draft: Erik Westphal
Writing – review & editing: Hermann Seitz

Ethics approval and consent to participate

Not applicable.

Consent for publication

Not applicable.

Availability of data

Data are available from the corresponding author on reasonable request.

References

1. Deutsches Institut für Normung, DIN EN ISO/ASTM 52900:2022-03, DIN Media GmbH, Berlin, 2022.

   doi: 10.31030/3290011

2. Westphal E. Digital Quality Assurance System for Additive Manufacturing Based on Machine Learning Methods and Blockchain Technology. Dissertation, University of Rostock, 2023.

   doi: 10.18453/ROSDOK_ID00004605

3. Wong KV, Hernandez A. A review of additive manufacturing. *ISRN Mech Eng.* 2012;2012:1-10.

   doi: 10.5402/2012/208760

4. Thompson Y, Gonzalez-Gutierrez J, Kukla C, Felfer P. Fused filament fabrication, debinding and sintering as a low cost

additive manufacturing method of 316L stainless steel. *Addit Manuf.* 2019;30:100861.

doi: 10.1016/j.addma.2019.100861

5. Mitteramskogler G, Gmeiner R, Felzmann R, *et al.* Light curing strategies for lithography-based additive manufacturing of customized ceramics. *Addit Manuf.* 2014;1-4:110-118.

doi: 10.1016/j.addma.2014.08.003

6. Spierings AB, Schneider M, Eggenberger R. Comparison of density measurement techniques for additive manufactured metallic parts. *Rapid Prototyp J.* 2011;17(5):380-386.

doi: 10.1108/13552541111156504

7. Slotwinski JA, Garboczi EJ, Hebenstreit KM. Porosity measurements and analysis for metal additive manufacturing process control. *J Res Natl Inst Stand Technol.* 2014;119:494-528.

doi: 10.6028/jres.119.019

8. Flodberg G, Pettersson H, Yang L. Pore analysis and mechanical performance of selective laser sintered objects. *Addit Manuf.* 2018;24:307-315.

doi: 10.1016/j.addma.2018.10.001

9. Bland S, Aboulkhair NT. Reducing porosity in additive manufacturing. *Met Powder Rep.* 2015;70(2):79-81.

doi: 10.1016/j.mprp.2015.01.002

10. Kruth JP, Levy G, Klocke F, Childs TH. Consolidation phenomena in laser and powder-bed based layered manufacturing. *CIRP Ann*. 2007;56(2):730-759.

doi: 10.1016/j.cirp.2007.10.004

11. Guddati S, Kiran ASK, Leavy M, Ramakrishna S. Recent advancements in additive manufacturing technologies for porous material applications. *Int J Adv Manuf Technol*. 2019;105(1-4):193-215.

doi: 10.1007/s00170-019-04116-z

12. Al-Maharma AY, Patil SP, Markert B. Effects of porosity on the mechanical properties of additively manufactured components: A critical review. *Mater Res Express.* 2020;7(12):122001.

doi: 10.1088/2053-1591/abcc5d

13. American Society for Testing and Materials, ASTM B276-21 - Standard Test Method for Apparent Porosity in Cemented Carbides, ASTM International, West Conshohocken, Pennsylvania, USA, 2023.

doi: 10.1520/B0276-21

14. Buffière JY, Savelli S, Jouneau PH, Maire E, Fougères R. Experimental study of porosity and its relation to fatigue mechanisms of model Al-Si7-Mg0.3 cast Al alloys. *Mater Sci Eng*. 2001;316(1-2):115-126.

doi: 10.1016/S0921-5093(01)01225-4

15. Damon J, Dietrich S, Vollert F, Gibmeier J, Schulze V. Process dependent porosity and the influence of shot peening on porosity morphology regarding selective laser melted AlSi10Mg parts. *Addit Manuf*. 2018;20:77-89.

doi: 10.1016/j.addma.2018.01.001

16. Heinl P, Müller L, Körner C, Singer RF, Müller FA. Cellular Ti-6Al-4V structures with interconnected macro porosity for bone implants fabricated by selective electron beam melting. *Acta Biomater.* 2008;4(5):1536-1544.

doi: 10.1016/j.actbio.2008.03.013

17. Wits WW, Carmignato S, Zanini F, Vaneker TH. Porosity testing methods for the quality assessment of selective laser melted parts. *CIRP Ann.* 2016;65(1):201-204.

doi: 10.1016/j.cirp.2016.04.054

18. Otto R, Kiener C, Küsters Y, Sørby K. Additive manufacturing of open porous functional structures: Roadmap from manufacturing to the application. *Procedia CIRP.* 2022;112:334-339.

doi: 10.1016/j.procir.2022.09.102

19. Deutsches Institut für Normung, DIN ISO 15901-1:2019-03, DIN Media GmbH, Berlin, 2019.

doi: 10.31030/3031674

20. Klobes P, Munro RG. *Porosity and Specific Surface Area Measurements for Solid Materials*; 2006. Available from: https://www.nist.gov/publications/porosity-and-specific-surface-area-measurements-solid-materials [Last accessed on 2025 Mar 20].

21. Arvieu C, Galy C, Le Guen E, Lacoste E. Relative density of SLM-produced aluminum alloy parts: Interpretation of results. *J Manuf Mater Process.* 2020;4(3):83.

doi: 10.3390/jmmp4030083

22. Dupin S, Lame O, Barrès C, Charmeau JY. Microstructural origin of physical and mechanical properties of polyamide 12 processed by laser sintering. *Eur Polym J.* 2012;48(9):1611-1621.

doi: 10.1016/j.eurpolymj.2012.06.007

23. Damon J, Dietrich S, Gorantla S, Popp U, Okolo B, Schulze V. Process porosity and mechanical performance of fused filament fabricated 316L stainless steel. *Rapid Prototyp J.* 2019;25(7):1319-1327.

doi: 10.1108/RPJ-01-2019-0002

24. Gong H, Snelling D, Kardel K, Carrano A. Comparison of stainless steel 316L parts made by FDM- and SLM-based additive manufacturing processes. *JOM.* 2019;71(3):880-885.

doi: 10.1007/s11837-018-3207-3

25. Caminero MÁ, Romero A, Chacón JM, Núñez PJ, García-Plaza E, Rodríguez GP. Additive manufacturing of 316L

stainless-steel structures using fused filament fabrication technology: Mechanical and geometric properties. *Rapid Prototyp J*. 2021;27(3):583-591.

doi: 10.1108/RPJ-06-2020-0120

26. Galarraga H, Lados DA, Dehoff RR, Kirka MM, Nandwana P. Effects of the microstructure and porosity on properties of Ti-6Al-4V ELI alloy fabricated by electron beam melting (EBM). *Addit Manuf*. 2016;10:47-57.

    doi: 10.1016/j.addma.2016.02.003

27. Scharowsky T, Juechter V, Singer RF, Körner C. Influence of the scanning strategy on the microstructure and mechanical properties in selective electron beam melting of Ti-6Al-4V. *Adv Eng Mater*. 2015;17(11):1573-1578.

    doi: 10.1002/adem.201400542

28. Homa J, Schwentenwein M. A novel additive manufacturing technology for high-performance ceramics. In: *Advanced Processing and Manufacturing Technologies for Nanostructured and Multifunctional Materials*. United States: John Wiley; 2014. p. 33-40.

    doi: 10.1002/9781119040354.ch4

29. Llanos G. *Additive Manufacturing of Zirconia: Chalmers University of Technology*; 2018. Available from: https://odr.chalmers.se/handle/20.500.12380/255513 [Last accessed on 2025 Mar 20].

30. Suominen JM, Frankberg EJ, Vallittu PK, *et al.* Three-dimensional printing of zirconia: Characterization of early stage material properties. *Biomater Invest Dent*. 2019;6(1):23-31.

    doi: 10.1080/26415275.2019.1640608

31. Pellegrini A, Palmieri ME, Guerra MG. Evaluation of anisotropic mechanical behaviour of 316L parts realized by metal fused filament fabrication using digital image correlation. *Int J Adv Manuf Technol*. 2022;120(11-12):7951-7965.

    doi: 10.1007/s00170-022-09303-z

32. O'Connor H, Singh G, Kumar A, Paetzold R, Celikin M, O'Cearbhaill ED. Fused filament fabrication using stainless steel 316L-polymer blend: Analysis and optimization for green density and surface roughness. *Polym Composites*. 2024;45(12):10632-10644.

    doi: 10.1002/pc.28496

33. Reddy PK, Gandhi P, Singh G. Additive manufacturing of yttria-stabilized zirconia using digital light processing: Green density and surface roughness analysis. *Ceram Int*. 2024;50(13):22974-22988.

    doi: 10.1016/j.ceramint.2024.04.021

34. Forward AM. *Technologies GmbH. Ultrafuse® 316L: Stainless Steel Composite Metal Filament for 3D Printers*. Available from: https://forward-am.com/material-portfolio/ultrafuse-filaments-for-fused-filaments-fabrication-fff/metal-filaments/ultrafuse-316l [Last accessed on 2024 Sep 04].

35. Lithoz GmbH. Thermal Post Processing - LithaCon 3Y 230. V2; TPP201.209. Unpublished thermal post processing data sheet, 2020.

36. Lithoz GmbH. Technical Data Sheet: LithaCon 3Y 230 D. Unpublished technical data sheet, 2019.

37. Hughes S, Quintero Olaya S. Using pycnometry and Archimedes' principle to measure the gross and air cavity volume of fruit. *IOP SciNotes*. 2021;2(2):25201.

    doi: 10.1088/2633-1357/abf33f

38. De Terris T, Andreau O, Peyre P, *et al.* Optimization and comparison of porosity rate measurement methods of selective laser melted metallic parts. *Addit Manuf*. 2019;28:802-813.

    doi: 10.1016/j.addma.2019.05.035

39. Kurose T, Abe Y, Santos MVA, *et al.* Influence of the layer directions on the properties of 316L stainless steel parts fabricated through fused deposition of metals. *Materials (Basel)*. 2020;13(11):2493.

    doi: 10.3390/ma13112493

40. Caminero MÁ, Romero Gutiérrez A, Chacón JM, García-Plaza E, Núñez PJ. Effects of fused filament fabrication parameters on the manufacturing of 316L stainless-steel components: Geometric and mechanical properties. *Rapid Prototyp J*. 2022;28(10):2004-2026.

    doi: 10.1108/RPJ-01-2022-0023

41. Rosnitschek T, Seefeldt A, Alber-Laukant B, Neumeyer T, Altstädt V, Tremmel S. Correlations of geometry and infill degree of extrusion additively manufactured 316L stainless steel components. *Materials (Basel)*. 2021;14(18):5173.

    doi: 10.3390/ma14185173

42. BASF 3D Printing Solutions GmbH. *Ultrafuse® Metal Filaments: User Guidelines for 3D Printing Metal Parts*. Available from: https://forward-am.com/material-portfolio/ultrafuse-filaments-for-fused-filaments-fabrication-fff/metal-filaments/ultrafuse-316l [Last accessed on 2023 Apr 27].

43. MBF Bioscience. *Glossary: Stereology Terms Stereology Information Center*. Available from: https://www.stereology.info/glossary-terms [Last accessed on 2023 Apr 27].

44. Carazzone JR, Martin CL, Cordero ZC. Crack initiation, propagation, and arrest in sintering powder aggregates. *J Am Ceram Soc*. 2020;103(9):4754-4773.

    doi: 10.1111/jace.17170